Vol 18 No 6, June 2009
1674-1056/2009/18(06)/2250-08

Chinese Physics B

© 2009 Chin. Phys. Soc.
and IOP Publishing Ltd

Elastic collisions between Si and D atoms at low temperatures and accurate analytic potential energy function and molecular constants of the SiD($X^2\Pi$) radical*

Shi De-Heng(施德恒)[a)b)†], Zhang Jin-Ping(张金平)[b)],
Sun Jin-Feng(孙金锋)[a)], and Zhu Zun-Lue(朱遵略)[a)]

[a)] *College of Physics & Information Engineering, Henan Normal University, Xinxiang* 453007, *China*

[b)] *College of Physics & Electronic Engineering, Xinyang Normal University, Xinyang* 464000, *China*

(Received 12 July 2008; revised manuscript received 20 November 2008)

Interaction potential of the SiD($X^2\Pi$) radical is constructed by using the CCSD(T) theory in combination with the largest correlation-consistent quintuple basis set augmented with the diffuse functions in the valence range. Using the interaction potential, the spectroscopic parameters are accurately determined. The present D_0, D_e, R_e, ω_e, α_e and B_e values are of 3.0956 eV, 3.1863 eV, 0.15223 nm, 1472.894 cm^{-1}, 0.07799 cm^{-1} and 3.8717 cm^{-1}, respectively, which are in excellent agreement with the measurements. A total of 26 vibrational states is predicted when $J = 0$ by solving the radial Schrödinger equation of nuclear motion. The complete vibrational levels, classical turning points, initial rotation and centrifugal distortion constants when $J = 0$ are reported for the first time, which are in good accord with the available experiments. The total and various partial-wave cross sections are calculated for the elastic collisions between Si and D atoms in their ground states at 1.0×10^{-11}–1.0×10^{-3} a.u. when the two atoms approach each other along the SiD($X^2\Pi$) potential energy curve. Four shape resonances are found in the total elastic cross sections, and their resonant energies are of 1.73×10^{-5}, 4.0×10^{-5}, 6.45×10^{-5} and 5.5×10^{-4} a.u., respectively. Each shape resonance in the total elastic cross sections is carefully investigated. The results show that the shape of the total elastic cross sections is mainly dominated by the s partial wave at very low temperatures. Because of the weakness of the shape resonances coming from the higher partial waves, most of them are passed into oblivion by the strong s partial-wave elastic cross sections.

Keywords: elastic collision, total cross section, shape resonance, spectroscopic parameter
PACC: 3440, 3120C, 3520G

1. Introduction

SiH and SiD are two free radicals of fundamental importance. This is because, on the one hand, as chemical intermediates, the two radicals play an important role in many industrial processes, such as plasma vapor deposition, thin film formation and semiconductor manufacturing.[1,2] On the other hand, the SiH radical has already been identified in the spectra of sunspots,[3,4] which gives us a strong clue that it is possible for the SiD radical to exist in such places. For these reasons, researchers have paid much attention to them in recent years.

However for the SiD($X^2\Pi$) radical, to our surprise, the extracted spectroscopic properties are all incomplete, both theoretically and experimentally. For example, in theory, we have not found any calculations about its vibrational manifolds, which are very useful in the rovibrational transition calculations. And since the elastic collision properties, such as the total and various partial-wave cross sections, are very sensitive to the interaction potential, no investigations can be found about the elastic collisions between Si and D atoms in their ground states in the cold regime due to the lack of accurate analytic potential energy function (APEF). In experiment, thus far the accurate dissociation energy has not been determined. All these motivate us to perform the present investigations.

One of the present purposes is to construct the reliable interaction potential of the SiD($X^2\Pi$) radical.

*Project supported by the National Natural Science Foundation of China (Grant Nos 60777012 and 10574039) and the Program for Science & Technology Innovation Talents in Universities of Henan Province in China (Grant No 2008HASTIT008).
†E-mail: scattering@sina.com.cn

In the next Section, we briefly describe the theory of low-energy elastic scattering. In Section 3, we determine the accurate APEF, derive the spectroscopic parameters and calculate the vibrational manifolds. In Section 4, we investigate the total and various partial-wave cross sections for the elastic collisions between Si and D atoms in their ground states at low temperatures when two atoms approach each other along the SiD($X^2\Pi$) potential energy curve (PEC). Concluding remarks are made in Section 5. Atomic units are used throughout this paper unless otherwise specified.

2. Theory

In the centre-of-mass coordinate system, the radial Schrödinger equation for a two-atoms colliding system can be written as,[5,6]

$$\frac{\mathrm{d}^2u_l}{\mathrm{d}r^2}+\left[k^2-\frac{2\mu V(r)}{\hbar^2}-\frac{l(l+1)}{r^2}\right]u_l(r)=0. \quad (1)$$

Here u_l is the radial solution of the l-th partial-wave equation. r is the internuclear distance of two atoms. μ is the reduced mass of the colliding system. k is the wave number, which is determined in terms of the energy E of relative motion by $k^2=2\mu E/\hbar^2$. $V(r)$ is the diatomic interaction potential. The solution must be regular and behave asymptotically as the following formula when $r\to\infty$,

$$u_l(r)\sim A_l[\mathrm{j}_l(kr)+\tan\delta_l\mathrm{n}_l(kr)], \quad (2)$$

where j_l and n_l are the spherical Bessel and Neumann functions, respectively. A_l is an arbitrary amplitude. And δ_l is the scattering phase shift of the l-th partial wave. Alternatively, we can write

$$u_l(r)\sim A_l\sin\left(kr-\frac{1}{2}l\pi+\delta_l\right). \quad (3)$$

If A_l is chosen to be equal to unity, the solution $u_l(r)$ satisfies the following integral equation,[7]

$$\tan\delta_l=\frac{-2\mu}{\hbar^2k}\int_0^\infty \mathrm{j}_l(kr)V(r)u_l(r)\mathrm{d}r. \quad (4)$$

When l is equal to 0, 1, 2, ... , the scattering waves are usually called s partial wave, p partial wave, d partial wave, ... , respectively. The elastic cross section of the l-th partial wave, $\sigma_l(E)$, is defined by[8]

$$\sigma_l(E)=\frac{4\pi}{k^2}\cdot(2l+1)\sin^2\delta_l. \quad (5)$$

Then, the total elastic cross section, $\sigma_\mathrm{T}(E)$, can be calculated as

$$\sigma_\mathrm{T}(E)=\sum_{l=0}^{\infty}\sigma_l(E)=\frac{4\pi}{k^2}\sum_{l=0}^{\infty}(2l+1)\sin^2\delta_l. \quad (6)$$

With the accurate diatomic interaction potential derived from Gaussian 03 program package,[9] the $u_l(r)$ can be obtained by numerically solving the radial Schrödinger equation (1). Once the $u_l(r)$ is determined, various partial-wave cross sections for the elastic collisions of the ground-state Si and D atoms in the cold regime can be calculated according to equations (5) and (6).

3. Interaction potential

Here, we use the coupled-cluster singles-doubles-approximate-triples [CCSD(T)] theory[10] to study the harmonic frequency ω_e, the equilibrium internuclear distance R_e and the dissociation energy D_e of the SiD($X^2\Pi$) radical. For calculations of this kind, this theory has been proved particularly successful. In particular in recent years, a number of high-quality results have been reported for a variety of molecules.[11−14] The calculations are made in the Gaussian 03 program package[9] at a series of correlation-consistent basis sets, cc-pVnZ (n = 2, 3, 4, 5), of Dunning *et al*[15−18] in the valence range. Furthermore, the effects on the spectroscopic parameters by these basis sets augmented with the diffuse functions, aug-cc-pVnZ, are also investigated. The D_e, R_e and ω_e are all tabulated in Table 1. Here, it is to be noted that the D_e is calculated directly from the Gaussian 03 program package.

Table 1. The equilibrium parameters for the SiD($X^2\Pi$) radical at the CCSD(T) level of theory and the different correlation-consistent basis sets, cc-pVnZ and aug-cc-pVnZ.

basis sets	D_e/eV	R_e/nm	ω_e/cm^{-1}	basis sets	D_e/eV	R_e/nm	ω_e/cm^{-1}
cc-pVDZ	2.8787	0.15403	1454.642	aug-cc-pVDZ	2.9295	0.15432	1436.339
cc-pVTZ	3.0914	0.15289	1460.896	aug-cc-pVTZ	3.1169	0.15289	1459.270
cc-pVQZ	3.1599	0.15238	1471.952	aug-cc-pVQZ	3.1689	0.15244	1469.294
cc-pV5Z	3.1816	0.15224	1472.300	aug-cc-pV5Z	3.1863	0.15223	1472.894

The correlation-consistent basis sets are designed for correlation of the valence electrons. The cardinal number n determines the flexibility of the virtual excitation space. The basis set cc-pVnZ contains $(n+1)\times(n+1.5)\times(n+2)/3$ atomic orbitals. In these sets, atomic energy-optimized orbitals are added to the basis, from the beginning of cc-pVDZ, one shell at a time in the sense of the principal expansion. Thus in general, at the same hierarchy of the coupled-cluster theory, the larger the cardinal number n, the smaller the D_e, R_e and ω_e differences should be between the calculations and the experiments.[19] These can be clearly seen in Table 1. Therefore, further calculations are carried out at the aug-cc-pV5Z basis set. Here, to be convenient for comparison, D_e, R_e and ω_e results obtained at this basis set together with the experiments[19] and other theories[20] are collected in Table 2.

Table 2. Spectroscopic parameter comparison with the measurements for the SiD($X^2\Pi$) radical at the CCSD(T)/aug-cc-pV5Z level of theory.

source	D_0/eV	D_e/eV	R_e/nm	ω_e/cm^{-1}	B_e/cm^{-1}	α_e/cm^{-1}
this work	3.0956	3.1863	0.15223	1472.894	3.8717	0.07799
exp.[19]	≤3.0986	≤3.1885	0.15199	1469.32	3.8840	0.0781
theory[20]	—	—	—	1470.75	—	0.080

In general, the PEC calculations are carried out at intervals of 0.02 nm over the internuclear separation range from 0.072 to 2.48 nm. Only near the equilibrium position, the interval is of 0.01 nm. The *ab initio* calculation points are fitted to the Murrell–Sorbie (M–S) function,[21]

$$V(\rho) = -D_e(1 + \sum_{i=1}^{n} a_i\rho^i)\exp(-a_1\rho), \qquad (7)$$

where, $\rho = r - R_e$, r is the diatomic internuclear distance. R_e is its equilibrium internuclear distance and is regarded as a fixed parameter in the fitting process. The D_e and the parameters a_i (i = 1, 2, ... , n) are determined by fitting.

Fitting equation (1) by the least-square method, the parameters a_i and D_e are obtained. In order to obtain a satisfactory result, of which the root-means square error is minimized, we try it from n = 3 to n = 8 and find that the best results can be obtained at n = 6. The fitting results are collected in Table 3 together with the R_e value for integrality.

Table 3. The parameters of the M–S APEF for the SiD($X^2\Pi$) radical at the CCSD(T)/aug-cc-pV5Z level of theory.

D_e/eV	R_e/nm	a_1/nm^{-1}	a_2/nm^{-2}	a_3/nm^{-3}	a_4/nm^{-4}	a_5/nm^{-5}	a_6/nm^{-6}	ΔE_{RMSE}/eV
3.1863	0.15223	26.0782	109.3513	421.5501	–5403.9456	–26297.174	112274.557	0.000895

By comparing the D_e value tabulated in Tables 1 and 2, it is not difficult to see that the one calculated directly from the Gaussian 03 program package is equal to the one obtained by the fitting. It indicates that the present fitting program is reliable and the fitting results are accurate. To further evaluate the fitting quality of the PEC, we calculate the root mean square error (ΔE_{RMSE}),

$$\Delta E_{RMSE} = \sqrt{\frac{1}{N}\left[\sum_{i=1}^{N}(V_{APEF} - V_{ab\ initio})^2\right]}. \qquad (8)$$

where $V_{APEF}(i)$ and $V_{ab\ initio}(i)$ are energies of the i-th point attained by the fitting and by the *ab initio* calculations, respectively. N is the number of fitting points (here N = 144). The present ΔE_{RMSE} is of only 0.000895 eV (about 0.2067 Kcal/mol). Obviously, our fitting accuracy about the APEF is greatly superior to the chemical accuracy (1.0 Kcal/mol).[22] This result further proves that the M-S function is very suitable for reproducing the PEC of this state, and the fitting process is of high quality.

Based on the relationships between the spectro-

scopic parameters and the M-S APEF,[23] the spectroscopic parameters, B_e, α_e and D_0, are calculated. In order to be conveniently compared with the measurements and other theories, these results are tabulated in Table 2, too.

From Table 2, it is easy to find that the R_e, ω_e, B_e and α_e values are in excellent agreement with the only measurements.[19] Their deviations between theory and experiment are of only 0.16%, 0.24%, 0.32% and 0.14%, respectively. At the same time, both D_0 and D_e are very close to the experiments.[19] According to these, we can further conclude that the present APEF is accurate.

Up to date, only the Kalemos group[20] have investigated the spectroscopic parameters of the SiD radical by employing the multireference configuration interaction (MRCI) approach. In their calculations, the aug-cc-pV6Z basis set for Si and the cc-pV5Z basis set for D atoms were used. However, they did not calculate the D_e values and did not give the expression of the APEF. At the same time, they did not determine the vibrational manifolds, which are very useful in the theoretical rovibrational transition calculations. Therefore, the present investigation is the most complete one about the SiD($X^2\Pi$) radical when compared with previous theories

In order to obtain the vibrational eigenvalues, we must solve the radial Schrödinger equation of nuclear motion. In the adiabatic approximation, the radial equation can be written as

$$\left[-\frac{\hbar^2}{2\mu}\frac{\mathrm{d}^2}{\mathrm{d}r^2}+\frac{\hbar^2}{2\mu r^2}J(J+1)+V(r)\right]\Psi_{\nu,J}(r) = E_{\nu,J}\,\Psi_{\nu,J}(r). \tag{9}$$

Here $V(r)$ is the adiabatic rotationless APEF tabulated in Table 3. r is the internuclear distance of the two atoms, Si and D. μ is the reduced mass of the SiD radical. ν and J are the vibrational and the rotational quantum numbers, respectively. $E_{\nu,J}$ and $\Psi_{\nu,J}(r)$ are the eigenvalues and eigenfunctions of the potential $J(J+1)\cdot\hbar^2/2\mu r^2+V(r)$, respectively. The rotational sublevel of a given vibrational level is represented by the following power series,[24]

$$\begin{aligned}E_{\nu,J} = {} & G(\nu)+B_\nu[J(J+1)]-D_\nu[J(J+1)]^2 \\ & +H_\nu[J(J+1)]^3+L_\nu[J(J+1)]^4 \\ & +M_\nu[J(J+1)]^5+N_\nu[J(J+1)]^6 \\ & +O_\nu[J(J+1)]^7.\end{aligned} \tag{10}$$

Here, $G(\nu)$ is the vibrational level. B_ν is the inertial rotation constant. D_ν, H_ν, L_ν, M_ν, N_ν and O_ν are the centrifugal distortion constants. By solving equation (9) numerically, we have obtained a total of 26 vibrational states for SiD($X^2\Pi$) when $J=0$. For each vibrational state, 1 vibrational level, 1 inertial rotation constant and 6 centrifugal distortion constants are obtained. Here, the vibrational levels, the classical turning points and the inertial rotation constants are all collected in Table 4, and the centrifugal distortion constants are all tabulated in Table 5.

Table 4. Vibrational levels, classical turning points and inertial rotation constants of SiD($X^2\Pi$) when $J=0$ at the CCSD(T)/aug-cc-pV5Z level of theory.

ν	$G(\nu)/\mathrm{cm}^{-1}$	$R_{\min}$/nm	$R_{\max}$/nm	B_ν/cm^{-1}	ν	$G(\nu)/\mathrm{cm}^{-1}$	$R_{\min}$/nm	$R_{\max}$/nm	B_ν/cm^{-1}
0	726.248	0.14201	0.16431	3.831889	13	16661.486	0.11398	0.24817	2.833560
1	2151.995	0.13555	0.17453	3.753339	14	17641.423	0.11317	0.25433	2.751009
2	3544.785	0.13154	0.18236	3.675979	15	18582.205	0.11243	0.26070	2.666035
3	4904.788	0.12852	0.18925	3.599555	16	19482.459	0.11175	0.26733	2.578136
4	6232.054	0.12608	0.19564	3.523823	17	20340.592	0.11111	0.27427	2.486700
5	7526.528	0.12401	0.20192	3.448543	18	21154.741	0.11053	0.28161	2.390958
6	8788.049	0.12223	0.20761	3.373479	19	21922.700	0.11000	0.28945	2.289916
7	10016.356	0.12066	0.21339	3.298396	20	22641.817	0.10952	0.29793	2.182232
8	11211.089	0.11926	0.21910	3.223058	21	23308.818	0.10908	0.30722	2.066014
9	12371.790	0.11780	0.22480	3.147222	22	23919.554	0.10869	0.31764	1.938416
10	13497.901	0.11685	0.23052	3.070636	23	24468.493	0.10834	0.32965	1.794777
11	14588.759	0.11581	0.23630	2.993029	24	24947.733	0.10804	0.34417	1.626377
12	15643.586	0.11486	0.24217	2.914112	25	25344.444	0.10780	0.36329	1.412435

Table 5. The centrifugal distortion constants for the SiD($X^2\Pi$) radical at the CCSD(T)/aug-cc- pV5Z level of theory when $J = 0$.

ν	$D_\nu(\times10^{-5})/\mathrm{cm}^{-1}$	$H_\nu(\times10^{-10})/\mathrm{cm}^{-1}$	$L_\nu(\times10^{-14})/\mathrm{cm}^{-1}$	$M_\nu(\times10^{-19})/\mathrm{cm}^{-1}$	$N_\nu(\times10^{-23})/\mathrm{cm}^{-1}$	$O_\nu(\times10^{-27})/\mathrm{cm}^{-1}$
0	10.80896	21.37909	–4.450527	8.932086	–8.621186	2.679273
1	10.62681	20.88671	–5.016582	9.409012	–8.244005	2.447399
2	10.46312	20.28868	–5.528124	9.840887	–8.367746	2.030752
3	10.31832	19.59767	–6.000801	10.03360	–8.972955	1.449181
4	10.19280	18.82080	–6.453089	9.815143	–10.07044	0.655356
5	10.08698	17.95974	–6.906136	9.013798	–11.72178	–0.467465
6	10.00140	17.01056	–7.384279	7.432850	–14.06300	–2.122783
7	9.936796	15.96341	–7.916251	4.819475	–17.33833	–4.641715
8	9.894160	14.80172	–8.537253	0.822817	–21.95429	–8.560774
9	9.874859	13.50093	–9.292184	–5.067110	–28.57148	–14.76927
10	9.880740	12.02638	–10.24061	–13.61428	–38.26384	–24.77691
11	9.914277	10.33008	–11.46450	–25.99093	–52.80303	–41.22854
12	9.978774	8.345720	–13.08044	–44.03881	–75.17996	–68.90988
13	1.007865	5.980862	–15.25969	–70.72784	–110.5956	–116.8021
14	10.21982	3.104642	–18.26197	–110.9938	–168.4194	–202.4704
15	1.041036	–0.472311	–22.49468	–173.3345	–266.2498	–361.9594
16	1.066137	–5.031641	–28.62143	–273.0065	–438.8052	–673.4999
17	10.98849	–11.00655	–37.77107	–438.8062	–758.7133	–1318.642
18	11.41439	–19.09126	–51.96549	–728.4898	–1389.080	–2754.394
19	11.97310	–30.45600	–75.06187	–1266.925	–2729.819	–6253.003
20	12.71811	–47.20351	–115.0269	–2351.028	–5877.222	–15841.65
21	13.73893	–73.43922	–190.1126	–4780.776	–14312.71	–46629.48
22	15.19842	–118.1376	–348.5097	–11116.55	–41593.62	–170479.3
23	17.43131	–204.4162	–746.9302	–31939.31	–159410.2	–877051.5
24	21.27334	–409.9517	–2104.461	–134544.6	–1009582	–8434631
25	29.76544	–1183.308	–11334.82	–1453671	-2.26145×10^7	-4.03770×10^8

In experiment, little information about the vibrational manifolds can be found in the literature.[25]To our knowledge, only the inertial rotation constant (B_ν) and the centrifugal distortion constant (D_ν) are available when the energy level is lower than two. In order to keep the clarity of Tables 4 and 5, we separately tabulate them in Table 6. By the B_ν comparison between theories and experiments,[25] it is easy to find that the largest deviation does not exceed 0.38%. And by the D_ν comparison between theories and experiments,[25] it is not difficult to calculate that the largest deviation does not exceed 0.98%.

Table 6. The B_ν and D_ν experimental results[25] of the SiD($X^2\Pi$) radical for $\nu = 0$, 1 when $J = 0$.

	$\nu = 0$	$\nu = 1$		$\nu = 0$	$\nu = 1$
B_ν/cm^{-1}	3.846656	3.765807	$D_\nu(\times10^{-4})/\mathrm{cm}^{-1}$	1.0916	1.0656

We have used the present program codes to calculate the vibrational levels, inertial rotation and centrifugal distortion constants of a number of molecules, such as the CH($X^2\Pi$) radical,[14] the ND($X^3\Sigma^-$) radical,[26] the SH($X^2\Pi$) radical[27] and the $^7Li_2(X^1\Sigma_g^+)$ dimer.[28] Favorable agreement is obtained when these results are compared with the available RKR data. These investigations show that the present method is reliable and accurate.

Unfortunately, both theoretically and experimentally, we have not found any results about the vibrational levels, classical turning points, inertial rotation and centrifugal distortion constants for the SiD($X^2\Pi$) radical when the level is higher than one. Thus we cannot make any direct comparison. But according to the high-quality fitting process of the APEF, the remarkable agreement between the present spectroscopic parameters and

the experiments[19] and the excellent agreement between the theoretical vibrational manifolds and the available RKR data,[25] we have enough reasons to believe that the results collected in Tables 4 and 5 are accurate.

4. Total and partial-wave elastic cross sections

By solving equation (1) numerically, the radial wavefunction u_l can be obtained. In this paper, we use the Numerov method with the automatic step-size selection to solve this equation. The partial-wave phase shift δ_l of the elastic collisions between the ground-state atoms, Si and D, is calculated at low and ultralow temperatures according to the formula (4) when the two atoms approach each other along the SiD($X^2\Pi$) PEC. Various elastic partial-wave cross sections and the total elastic cross sections are calculated by equations (5) and (6) over the impact energy range from 1.0×10^{-11} to 1.0×10^{-3} a.u.. The collision energy dependence of the total elastic cross sections evaluated at low and ultralow temperatures is depicted in Fig.1. And the collision energy dependences of elastic cross sections for some selected partial waves are presented in Figs.2–4, respectively.

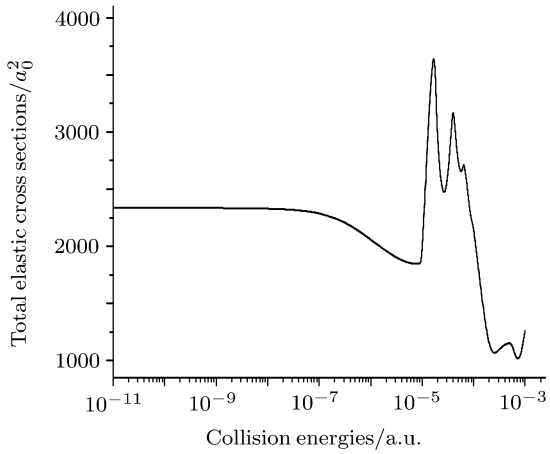


Fig.1. Total elastic cross sections versus collision energies for scattering along the potential energy curve of the SiD ground state.

As shown in Fig.1, the total cross sections of elastic collisions between two ground-state atoms, Si and D, are very large and are almost constant at very low temperatures. From Figs.2–4, we can see that the s partial-wave cross sections are significant when the collision energy is below 10^{-6} a.u., whereas the rest of the partial-wave cross sections are very small. Especially when the impact energy is lower than 10^{-7} a.u., we can clearly see that only the s partial wave has contributions to the total elastic cross sections. Therefore, the total elastic cross sections are dominated by s-wave scattering at this energy range. With the energy increasing, the s-wave cross sections tend to decrease, but the decrease is obviously overcome by the higher partial-wave contributions. Particularly when the impact energy is higher than 10^{-5} a.u., the significance of the higher partial waves greatly extrudes. Therefore, as shown in Fig.1, some resonant peaks occur by the addition of the higher partial waves. Incidentally, only a very weak shape resonance is found in the s wave cross sections, and the resonant energy is determined at 3.64×10^{-5} a.u..

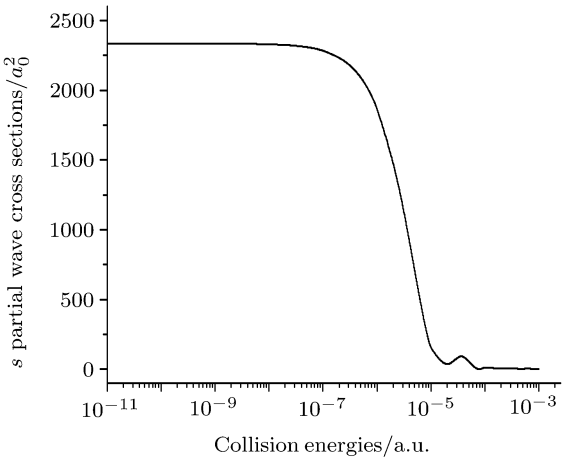


Fig.2. s partial wave cross sections versus collision energies for scattering along the potential energy curve of the SiD ground state.

Four shape resonances are found in the total elastic cross sections. Obviously, these peaks come from the shape resonances. At very low temperatures, with the collision energy increasing, the first sharp resonant peak appears. Careful calculations tell us that it results from the $l = 2$, 5 partial wave contributions and the resonant energy is of 1.73×10^{-5} a.u.. Subsequently, the second peak arrives. The peak is consistent with the resonant position of the $l = 2$ and 6 partial waves and the resonant energy is of 4.0×10^{-5} a.u.. For the third shape resonance, investigations have shown that its most prominent composition comes from the $l = 1$ and 5 partial waves and the resonant energy is of 6.45×10^{-5} a.u.. The last shape resonance depicted in Fig.1 is of 5.5×10^{-4} a.u.,

it overlaps with the resonant position of the $l = 2$, 5, 11 and 18 partial waves.

As shown in Fig.3, a sharp resonant peak exists in the p partial wave, and its resonant energy is of 7.55×10^{-6} a.u.. Compared with the s partial wave, this shape resonance is too weak thus it is passed into oblivion by the strong s wave cross sections. The analyses are the same for most of the shape resonances coming from the higher partial waves.

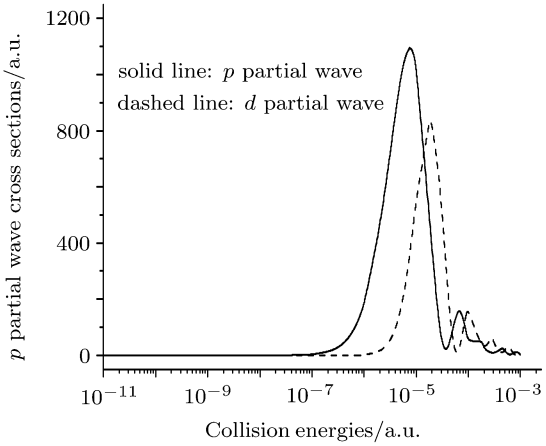


Fig.3. p and d partial wave cross sections versus collision energies for scattering along the potential energy curve of the SiD ground state.

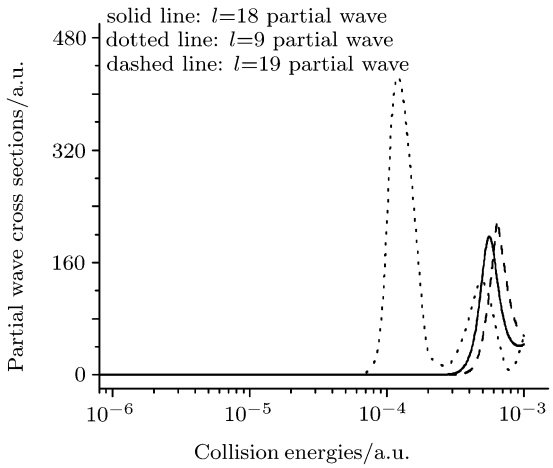


Fig.4. $l = 9$, 18 and 19 partial wave cross sections versus collision energies for scattering along the potential energy curve of the SiD ground state.

From Fig.1, it is not difficult to see that some of the resonant peaks are not sharp. The reason is that each shape resonance in Fig.1 is contributed by different partial waves. For a specified peak, such as the last shape resonance, only the resonant position of $l = 2$, 5, 11 and 18 partial waves superposes it. Some partial-wave peaks (such as the $l = 9$ and 19 partial waves) are slightly different from this position, as shown in Fig.4. Because of the slight different positions of these resonant peaks, their mutual overlapping broadens the shape resonance in the total cross sections, as demonstrated in Fig.1.

We have investigated the elastic collisions between two ground-state Li atoms at low and ultralow temperatures using the present theoretical method.[29] The results are in excellent agreement with the experiments. Thus, the present method should be reliable. Since the interaction potential attained here is accurate and reliable, therefore, though no experimental and theoretical results can be found about the elastic collisions between two Si and D atoms at low and ultralow temperatures, we should believe that the total and various elastic cross sections calculated in this paper are reliable and accurate. These results are expected to be detected experimentally and to be examined theoretically in the near future.

5. Conclusions

The interaction potential of the SiD($X^2\Pi$) radical is constructed by using the CCSD(T) theory in combination with the correlation-consistent quintuple basis set augmented with the diffuse functions in the valence range. Consequently, the spectroscopic parameters and the vibrational manifolds have been determined. Excellent agreement is found when compared with the available experiments. In contrast with previous experiments and theories, it is not difficult to find that the present work is more complete and accurate as a whole. Using the present interaction potential, the total and various elastic cross sections of two Si and D collisions are investigated for the first time when the two atoms approach each other along the SiD($X^2\Pi$) PEC. Four shape resonances are found in the total elastic cross sections, and their resonant energies are of 1.73×10^{-5}, 4.0×10^{-5}, 6.45×10^{-5} and 5.55×10^{-4} a.u., respectively. Each shape resonance in the total elastic cross sections is investigated in detail. The results show that the shape of the total elastic cross sections is mainly dominated by the s partial wave at very low temperatures. Because of the weakness of the shape resonances coming from the higher partial waves, most of them are passed into oblivion by the strong s partial-wave elastic cross sections.

References

[1] Turban G, Catherine Y and Grolleau B 1981 *Thin. Solid Films* **77** 287

[2] Jasinski J M, Becerra R and Walsh R 1995 *Chem. Rev.* **95** 1203

[3] Schadee A 1964 *Bull. Astron. Inst. Neth.* **17** 311

[4] Sauval A J 1969 *Solar Phys.* **10** 319

[5] Côté R and Dalgarno A 1994 *Phys. Rev.* A **50** 4827

[6] Shi D H, Zhang J P, Sun J F, Zhu Z L, Liu Y F and Yang X D 2008 *Chin. Phys.* B **17** 2090

[7] Côté R, Dalgarno A and Jamieson M J 1994 *Phys. Rev.* A **50** 399

[8] Jamieson M J, Dalgarno A and Yukich J N 1992 *Phys. Rev.* A **46** 6956

[9] Frisch M J, Trucks G W, Schlegel H B, Scuseria G E, Robb M A, Cheeseman J R, Jr Montgomery J A, Vreven T, Kudin K N, Burant J C, Millam J M, Iyengar S S, Tomasi J, Barone V, Mennucci B, Cossi M, Scalmani G, Rega N, Petersson G A, Nakatsuji H, Hada M, Ehara M, Toyota K, Fukuda R, Hasegawa J, Ishida M, Nakajima T, Honda Y, Kitao O, Nakai H, Klene M, Li X, Knox J E, Hratchian H P, Cross J B, Adamo C, Jaramillo J, Gomperts R, Stratmann R E, Yazyev O, Austin A J, Cammi R, Pomelli C, Ochterski J W, Ayala P Y, Morokuma K, Voth G A, Salvador P, Dannenberg J J, Zakrzewski V G, Dapprich S, Daniels A D, Strain M C, Farkas O, Malick D K, Rabuck A D, Raghavachari K, Foresman J B, Ortiz J V, Cui Q, Baboul A G, Clifford S, Cioslowski J, Stefanov B B, Liu G, Liashenko A, Piskorz P, Komaromi I, Martin R L, Fox D J, Keith T, Al-Laham M A, Peng C Y, Nanayakkara A, Challacombe M, Gill P M W, Johnson B, Chen W, Wong M W, Gonzalez C and Pople J A 2004 *Gaussian 03 Revision D.01* (Wallingford CT: Gaussian Inc.)

[10] Raghavachari K, Trucks G W, Pole J A and Head-Gordon M 1989 *Chem. Phys. Lett.* **157** 479

[11] Pawlowski F, Jørgensen P, Olsen J, Hegelund F, Helgaker T, Gauss J, Bak K L and Stanton J F 2002 *J. Chem. Phys.* **116** 6482

[12] Ruden T A, Taylor P R and Helgaker T 2003 *J. Chem. Phys.* **119** 1951

[13] Ruden T A, Helgaker T, Jørgensen P and Olsen J 2004 *J. Chem. Phys.* **121** 5874

[14] Shi D H, Zhang J P, Sun J F, Liu Y F, Zhu Z L and Yu B H 2008 *J. Mol. Struct.* (THEOCHEM) **860** 101

[15] Dunning T H 1989 *J. Chem. Phys.* **90** 1007

[16] Peterson K A, Woon D E and Dunning T H 1994 *J. Chem. Phys.* **100** 7410

[17] Woon D E and Dunning T H 1993 *J. Chem. Phys.* **99** 1914

[18] Peterson K A, Kendall R A and Dunning T H 1993 *J. Phys. Chem.* **99** 1930

[19] Huber K P and Herzberg G 1979 *Molecular Spectra and Molecular Structure* Vol.4 *Constants of Diatomic Molecules* (New York: Van Nostrand Reinhold) p600

[20] Kalemos A, Marridis A and Metropoulos A 2002 *J. Chem. Phys.* **116** 6529

[21] Murrell J N, Carter S, Farantos S C, Huxley P and Varandas J C 1984 *Molecular Potential Energy Functions* (Chichester: John Wiley & Sons) p9

[22] Aguado A and Paniagua M 1992 *J. Chem. Phys.* **96** 1265

[23] Yan S Y and Bao W S 2007 *Chin. Phys.* **16** 3675

[24] Herzberg G 1951 *Molecular Spectra and Molecular Structure*, Vol.1 (New York: Van Nostrand Reinhold) Chapt.3

[25] Ram R S, Engleman R and Bernath P F 1998 *J. Mol. Spectrosc.* **190** 341

[26] Shi D H, Zhang J P, Liu Y F, Sun J F and Zhu Z H 2008 *Int. J. Quantum Chem.* **109** 202

[27] Shi D H, Zhang J P, Sun J F, Liu Y F, Zhu Z L, Ma H and Yang X D 2008 *Chin. Phys.* B **17** 3678

[28] Shi D H, Sun J F, Zhu Z L, Ma H and Yang X D 2008 *Acta Phys. Sin.* **57** 165 (in Chinese)

[29] Sun J F, Zhang J C and Wang J M 2006 *Chin. Phys.* **15** 531